Electron–phonon interaction dressed by electronic correlations near charge ordering. Possible implications for cobaltates

2006 J. Phys.: Condens. Matter 18 11411

(http://iopscience.iop.org/0953-8984/18/50/002)

INSTITUTE OF PHYSICS PUBLISHING JOURNAL OF PHYSICS: CONDENSED MATTER

J. Phys.: Condens. Matter **18** (2006) 11411–11428 doi:10.1088/0953-8984/18/50/002

Electron–phonon interaction dressed by electronic correlations near charge ordering. Possible implications for cobaltates

A Foussats[1], A Greco[1], M Bejas[1,2] and A Muramatsu[2]

[1] Facultad de Ciencias Exactas, Ingeniería y Agrimensura and Instituto de Física Rosario (UNR-CONICET), Avenida Pellegrini 250-2000 Rosario, Argentina
[2] Institut für Theoretische Physik III, Universität Stuttgart, Pfaffenwaldring 57, D-70550 Stuttgart, Germany

E-mail: foussats@ifir.edu.ar and agreco@fceia.unr.edu.ar

Received 27 July 2006, in final form 4 October 2006
Published 27 November 2006
Online at stacks.iop.org/JPhysCM/18/11411

Abstract

We consider possible routes to superconductivity on the basis of the t–J–V model plus phonons on the triangular lattice. We studied the stability conditions for the homogeneous Fermi liquid (HFL) phase against different broken symmetry phases. Besides the $\sqrt{3} \times \sqrt{3}$ CDW phase, triggered by the nearest-neighbour Coulomb interaction V, we have found that the HFL is unstable, at very low doping, against a bond-ordered phase due to J. We also discuss the occurrence of phase separation at low doping and V. The interplay between the electron–phonon interaction and correlations near the $\sqrt{3} \times \sqrt{3}$ CDW leads to superconductivity in the unconventional next-nearest-neighbour f-wave (NNN-f) channel with a dome shape for T_c around $x \sim 0.35$, and with values of a few kelvin. Near the bond-ordered phase at low doping we found tendencies to superconductivity with d-wave symmetry for finite J and $x < 0.15$. Possible implications for cobaltates are discussed.

1. Introduction

Since superconductivity was discovered in hydrated cobaltates $Na_xCoO_2 \cdot yH_2O$ for $x \sim 0.35$ and $y \sim 1.3$ [1] an enormous amount of attention has been focused on this system, in spite of the rather modest critical temperature T_c, that follows a characteristic dome shape [2] with maximum value $T_c \sim 5$ K around a doping $x \sim 0.35$. Several proposals considered cobaltates as electron-doped Mott insulators with a layered structure, where Co ions are in a low-spin state ($S = 1/2$) on a triangular lattice. Following such arguments, it was expected that the resonating valence bond (RVB) scenario proposed long ago by Anderson [3] for the cuprates could be clearly realized in the cobaltates.

The importance of strong electronic correlations seems to be supported by several experiments. The small bandwidth of the (t_{2g}) levels close to the Fermi energy [4, 5] was

confirmed by recent photoemission studies [6, 7] showing for $x = 0.3$ a reduction of bandwidth by a factor of two with respect to the calculated ones [5]. In fact, even taking the whole t_{2g} manifold, the bare bandwidth is $\sim$1.6 eV [4], while from core level photoemission spectroscopy [8] values of the onsite interaction $U_{dd} \sim$ 3.0–5.5 eV were estimated. Hence, electronic correlations seem to play an essential role, so that Hubbard or t–J models were proposed [9] to describe cobaltates.

Several unconventional pairing channels and mechanisms were proposed for the superconducting state: (a) pure t–J model RVB based calculations predict singlet d-wave superconductivity [9–12] with time-reversal symmetry breaking; (b) charge fluctuations predict a triplet next-nearest-neighbour (NNN) f-wave state [13–15]; (c) spin-triplet f-wave superconductivity was also proposed based on phenomenology and symmetry considerations [16], due to the topology of the Fermi surface [17], from weak-coupling studies of a multiorbital Hubbard model [18], and considering spin–orbit coupling [19–21].

A number of magnetic resonance [22–24] and μSR [25, 26] experiments are consistent with unconventional triplet superconductivity and exclude time-reversal symmetry breaking [26]. Although those results seem at the moment not conclusive, with some NMR experiments [27] indicating the possibility for singlet s-wave superconductivity, specific heat measurements [28] are consistent with the existence of a superconducting gap with nodal lines. Based on the results pointing to triplet superconductivity with nodal lines, f-wave symmetry appears as a very promising candidate (see also [29] for a more detailed discussion).

Besides superconductivity, other features of the electronic structure point to the proximity of other instabilities. Photoemission spectroscopy indicates the presence of a pseudogap of $\sim$20 meV with a decrease of the density of states at the Fermi energy as the temperature is lowered [30]. Also Raman scattering experiments recently reported a pseudogap [31]. Sidebands in the spectra of E_{1g} phonons suggest that the pseudogap arises from a charge ordering instability. Such an instability was only observed in superconducting samples. A very recent photoemission experiment [32] was also interpreted in terms of the proximity of the system to a charge order phase. From the possible mechanisms for superconductivity discussed above, (b) reconciles the possibility of a charge ordering instability with an unconventional superconducting state characterized by nodal lines in the order parameter. However, estimates of T_c for a pure electronic model lead to extremely low values [14].

As a natural extension we have recently considered the interplay between phonons and electronic correlations [15]. There, the t–V model on the triangular lattice (where V is the Coulomb repulsion between nearest neighbours) was proposed for the electronic sub-system. The main effect of V is to bring the system closer to a $\sqrt{3} \times \sqrt{3}$ charge-density wave (CDW) phase where charge fluctuations are strongly increased. Under these circumstances, the electron–phonon (e–ph) interaction vertex is renormalized by charge fluctuations leading to superconductivity with NNN-f unconventional pairing symmetry around $x \sim 0.35$.

As mentioned above, originally, several theories were developed on the basis of the pure t–J model [9, 10, 12]. Moreover, recent NMR experiments [33] point to enhanced low frequency spin fluctuations before superconductivity sets in. Therefore, a more general study is needed, where both V as well as the antiferromagnetic spin exchange J are considered, in order to clarify the interplay or competition of electronic instabilities in different parts of the phase diagram.

We present here such a study, showing that the region where singlet d-wave pairing due to J dominates is well separated from the one where the NNN f-wave pairing appears.

The presence of J triggers a normal state V-independent instability at low doping. This so-called bond-order phase (BOP) is found to be mainly of d-wave character and dominated by the exchange interaction J. Phase separation (PS) was also obtained at low doping.

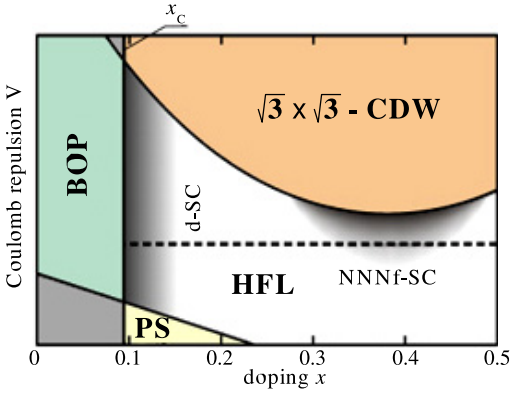

Figure 1. Sketch of the obtained generic phase diagram. The figure shows the phases HFL, BOP, $\sqrt{3} \times \sqrt{3}$ CDW and PS. Inside the HFL phase superconductivity is possible in the shading regions. Tendencies to superconductivity are larger in the regions where the intensity of the shadow is larger. For instance, making a cut at a given V along the dashed line we find superconductivity with NNN-f symmetry following a dome shape around $x \sim 0.38$. For low x superconductivity is possible with d-wave symmetry for finite J. With decreasing J the onset of the BOP (x_c) moves toward $x = 0$, and superconductivity is at the same time strongly suppressed. The diagram is presented for $0 < x < 0.5$, where our theory predicts superconducting phases.

(This figure is in colour only in the electronic version)

After identifying the parameter region (J–V–x) where the HFL is stable we have studied superconductivity. As in the case with $J = 0$, unconventional NNN-f pairing near the $\sqrt{3} \times \sqrt{3}$ CDW phase following a dome shape around $x \sim 0.35$ is obtained for expected values of J. The values for T_c obtained in the full model are of the order of a few kelvin. In addition, for finite J we have found tendencies to d-wave superconductivity in the immediate vicinity of the BOP. Figure 1 gives a sketch of the phase diagram obtained with our theory.

The paper is organized as follows. In section 2 the formalism used is summarized, in order to allow for a self-contained presentation. In section 3 the stability conditions for the homogeneous Fermi liquid (HFL) phase are discussed. Section 4 is devoted to superconductivity and its possible channels. In section 5, conclusions and discussions are presented.

2. A large-N approach for the t–J–V model and Feynman rules

Here we describe our treatment of the t–J–V model, given by

$$H = -t \sum_{\langle i,j\rangle,\sigma} (\tilde{c}^{\dagger}_{i\sigma} \tilde{c}_{j\sigma} + \text{h.c.}) + J \sum_{\langle i,j\rangle} (\vec{S}_i \vec{S}_j - \tfrac{1}{4} n_i n_j) + V \sum_{\langle i,j\rangle} n_i n_j \qquad (1)$$

where t, J and V are the hopping, the exchange interaction and the Coulomb repulsion, respectively, between nearest-neighbour sites denoted by $\langle ij\rangle$. $\tilde{c}^{\dagger}_{i\sigma}$ and $\tilde{c}_{i\sigma}$ are the fermionic creation and destruction operators of holes, respectively, under the constraint that double occupancy is excluded, and n_i is the corresponding density operator at site i.

Now, we introduce Hubbard operators [34] which are related to the fermionic operators as follows:

$$X_i^{\sigma 0} = \tilde{c}^{\dagger}_{i\sigma} \qquad n_i = (X_i^{\uparrow\uparrow} + X_i^{\downarrow\downarrow})$$
$$X_i^{0\sigma} = \tilde{c}_{i\sigma} \qquad X_i^{\uparrow\downarrow} = S_i^{+} \qquad X_i^{\downarrow\uparrow} = S_i^{-}.$$

The five operators $X_i^{\sigma\sigma'}$ and X_i^{00} are boson-like and the four operators $X_i^{\sigma 0}$ and $X_i^{0\sigma}$ are fermion-like. The names fermion-like and boson-like come from the fact that Hubbard operators do not verify the usual fermionic and bosonic commutations rules.

In previous papers [35–38] we have developed a large-N expansion for the t–J–V model in the framework of the path integral representation for the Hubbard X operators. In this approach the X-operators are treated as fundamental objects without any decoupling scheme, and hence, problems that arise in other treatments are avoided, like considering fluctuations of gauge fields that appear in the slave boson (SB) approach [39].

We start our formalism by extending the Hamiltonian of the t–J–V model, to N channels for the spin degrees of freedom, and rescaling couplings accordingly.

$$H = -\frac{t}{N}\sum_{\langle i,j\rangle,p}(\hat{X}_i^{p0}\hat{X}_j^{0p} + \text{h.c.}) + \frac{J}{2N}\sum_{\langle i,j\rangle;pp'}(\hat{X}_i^{pp'}\hat{X}_j^{p'p} - \hat{X}_i^{pp}\hat{X}_j^{p'p'}) + \frac{V}{N}\sum_{\langle i,j\rangle;pp'}\hat{X}_i^{pp}\hat{X}_j^{p'p'} - \mu\sum_{i,p}\hat{X}_i^{pp} \tag{2}$$

where the spin indices $\sigma, \bar{\sigma}$ were extended to new indices p and p' running from 1 to N. In order to obtain a finite theory in the infinite-N limit, we rescaled t, J and V as t/N, J/N and V/N, respectively. In (2) μ is the chemical potential.

As shown previously, a path integral can be obtained with an Euclidean Lagrangian L_{E} given by

$$L_{\text{E}} = \frac{1}{2}\sum_{i,p}\frac{(\dot{X}_i^{0p}X_i^{p0} + \dot{X}_i^{p0}X_i^{0p})}{X_i^{00}} + H \tag{3}$$

and the following two additional constraints:

$$X_i^{00} + \sum_p X_i^{pp} - \frac{N}{2} = 0 \tag{4}$$

and

$$X_i^{pp'} - \frac{X_i^{p0}X_i^{0p'}}{X_i^{00}} = 0, \tag{5}$$

which are required to satisfy the commutation rules of X-operators. While (4) is the completeness condition, (5) originates in the above mentioned requirement to satisfy the commutation rules. For a detailed discussion of the constraints, and their relation with the commutation rules, we refer to [35, 40]. In our path integral approach we associate Grassmann and usual bosonic variables with Fermi-like and boson-like X-operators, respectively.

We now discuss the main steps needed to introduce a large-N expansion [35, 37]. First, we integrate over the boson variables $X^{pp'}$ using (5). The completeness condition is enforced by exponentiating (4) and introducing Lagrange multipliers λ_i. We write the boson fields in terms of static mean-field values, (r_0, λ_0) and fluctuation fields δR_i, $\delta\lambda_i$, as

$$X_i^{00} = Nr_0(1 + \delta R_i) \qquad \lambda_i = \lambda_0 + \delta\lambda_i, \tag{6}$$

and we perform the following change of variables for the fermion fields:

$$f_{ip}^{\dagger} = \frac{1}{\sqrt{Nr_0}}X_i^{p0} \qquad f_{ip} = \frac{1}{\sqrt{Nr_0}}X_i^{0p}. \tag{7}$$

Due to (5), and after using (7), the exchange interaction contains four fermion fields that can be decoupled in terms of the bond variable Δ_{ij} through a Hubbard–Stratonovich transformation, where Δ_{ij} is the field associated with the quantity $\sum_p f_{jp}^{\dagger}f_{ip}/[(1+\delta R_i)(1+$

$\delta R_j)]^{1/2}$. We write the Δ_{ij} fields in term of static mean field values and dynamical fluctuations $\Delta_i^\eta = \Delta(1+r_i^\eta+\mathrm{i}A_i^\eta)$, where r_i^η and A_i^η correspond to the amplitude and the phase fluctuations of the bond variable, respectively. The index η takes three values associated with the bond directions $\eta_1 = (1, 0)$, $\eta_2 = (\frac{1}{2}, \frac{\sqrt{3}}{2})$ and $\eta_3 = (-\frac{1}{2}, \frac{\sqrt{3}}{2})$ of the triangular lattice.

Introducing the above change of variables, and after expanding $1/(1 + \delta R)$ in powers of δR, we arrive at the following effective Lagrangian:

$$\begin{aligned} L_{\mathrm{eff}} = &-\frac{1}{2}\sum_{i,p}\left(\dot{f}_{ip}f_{ip}^\dagger + \dot{f}_{ip}^\dagger f_{ip}\right)(1-\delta R_i+\delta R_i^2) + tr_0\sum_{\langle i,j\rangle,p}(f_{ip}^\dagger f_{jp}+\mathrm{h.c.}) \\ &-\mu\sum_{i,p}f_{ip}^\dagger f_{ip}(1-\delta R_i+\delta R_i^2) + N r_0\sum_i \delta\lambda_i\delta R_i + \sum_{i,p}f_{ip}^\dagger f_{ip}(1-\delta R_i)\delta\lambda_i \\ &+\frac{2N}{J}\Delta^2\sum_{i\eta}\left[(r_i^\eta)^2+(A_i^\eta)^2\right] + Nr_0^2\left(V-\frac{1}{2}J\right)\sum_{\langle i,j\rangle}\delta R_i\delta R_j \\ &-\Delta\sum_{\langle i,j\rangle,p}(f_{ip}^\dagger f_{jp}+f_{jp}^\dagger f_{ip})[1-\tfrac{1}{2}(\delta R_i+\delta R_j)+\tfrac{1}{4}\delta R_i\delta R_j \\ &+\tfrac{3}{8}(\delta R_i^2+\delta R_j^2)] - \Delta\sum_{\langle i,j\rangle,p,\eta}[f_{ip}^\dagger f_{jp}(r_i^\eta+\mathrm{i}A_i^\eta)[1-\tfrac{1}{2}(\delta R_i+\delta R_j)]+\mathrm{h.c.}], \end{aligned} \tag{8}$$

where we have changed μ to $\mu - \lambda_0$ and dropped constant and linear terms in the fields.

Looking at the effective Lagrangian (8), the Feynman rules can be obtained as usual. The bilinear parts give rise to the propagators and the remaining pieces are represented by vertices.

To leading order in $1/N$, we associate with the N-component fermion field f_p a propagator connecting two generic components p and p',

$$G_{pp'}^{(0)}(\mathbf{k}, \nu_n) = -\frac{\delta_{pp'}}{\mathrm{i}\nu_n - E_k} \tag{9}$$

which is of $\mathcal{O}(1)$ and where E_k is

$$E_k = -2(tr_0+\Delta)\left(\cos k_x + 2\cos\frac{k_x}{2}\cos\frac{\sqrt{3}}{2}k_y\right) - \mu, \tag{10}$$

and $\mathbf{k}$ and ν_n are the momentum and the fermionic Matsubara frequency of the fermionic field, respectively. The fermion variables f_{ip} are proportional to the X-operators (7) and should not be associated with the spinons from the SB approach.

The mean field values r_0 and Δ must be determined by minimizing the leading order theory. From the completeness condition (4) r_0 is equal to $x/2$, where x is the electron doping away from half-filling. On the other hand, the expression for Δ is

$$\Delta = \frac{J}{2N_\mathrm{s}}\frac{1}{3}\sum_{k,\eta}\cos(k_\eta)n_\mathrm{F}(E_k), \tag{11}$$

where n_F is the Fermi function and N_s is the number of sites in the lattice. For a given doping x; μ and Δ must be determined self-consistently from $(1-x) = \frac{2}{N_\mathrm{s}}\sum_k n_\mathrm{F}(E_k)$ and (11).

We associate with the eight-component boson field

$$\delta X^a = (\delta R, \delta\lambda, r^{\eta_1}, r^{\eta_2}, r^{\eta_3}, A^{\eta_1}, A^{\eta_2}, A^{\eta_3}),$$

the inverse of the propagator, connecting two generic components a and b,

$$D^{-1}_{(0)ab}(\mathbf{q},\omega_n) = N \begin{pmatrix} \gamma_q & x/2 & 0 & 0 & 0 & 0 & 0 & 0 \\ x/2 & 0 & 0 & 0 & 0 & 0 & 0 & 0 \\ 0 & 0 & \frac{4}{J}\Delta^2 & 0 & 0 & 0 & 0 & 0 \\ 0 & 0 & 0 & \frac{4}{J}\Delta^2 & 0 & 0 & 0 & 0 \\ 0 & 0 & 0 & 0 & \frac{4}{J}\Delta^2 & 0 & 0 & 0 \\ 0 & 0 & 0 & 0 & 0 & \frac{4}{J}\Delta^2 & 0 & 0 \\ 0 & 0 & 0 & 0 & 0 & 0 & \frac{4}{J}\Delta^2 & 0 \\ 0 & 0 & 0 & 0 & 0 & 0 & 0 & \frac{4}{J}\Delta^2 \end{pmatrix}, \tag{12}$$

where $\gamma_q = (4V - 2J)(x/2)^2\,(\cos k_x + 2\cos\frac{k_x}{2}\cos\frac{\sqrt{3}}{2}k_y)$ and the indices a, b run from 1 to 8. $\mathbf{q}$ and ω_n are the momentum and the Bose Matsubara frequency of the boson field, respectively.

The first component δR of the δX^a field is connected with charge fluctuations (6), i.e. $X^{00}_i = Nr_0(1 + \delta R_i)$, where X^{00} is the Hubbard operator associated with the number of electrons.

The non-quadratic terms in (8) define three- and four-leg vertices.

The three-leg vertex

$$\begin{aligned}\Lambda^{pp'}_a = (-1)\Bigg[&\frac{\mathrm{i}}{2}(\nu_n + \nu'_n) + \mu + 2\Delta\sum_\eta \cos\left(k_\eta - \frac{q_\eta}{2}\right)\cos\frac{q_\eta}{2}, 1, \\ &-2\Delta\cos\left(k_{\eta_1} - \frac{q_{\eta_1}}{2}\right), -2\Delta\cos\left(k_{\eta_2} - \frac{q_{\eta_2}}{2}\right), \\ &-2\Delta\cos\left(k_{\eta_3} - \frac{q_{\eta_3}}{2}\right), 2\Delta\sin\left(k_{\eta_1} - \frac{q_{\eta_1}}{2}\right), \\ &2\Delta\sin\left(k_{\eta_2} - \frac{q_{\eta_2}}{2}\right), 2\Delta\sin\left(k_{\eta_3} - \frac{q_{\eta_3}}{2}\right)\Bigg]\delta^{pp'}\end{aligned} \tag{13}$$

represents the interaction between two fermions and one boson.

The four-leg vertex $\Lambda^{pp'}_{ab}$ represents the interaction between two fermions and two bosons. The only elements different from zero are

$$\begin{aligned}\Lambda^{pp'}_{\delta R\delta R} = &\left(\frac{\mathrm{i}}{2}(\nu_n + \nu'_n) + \mu + \Delta\sum_\eta \cos\left(k_\eta - \frac{q_\eta + q'_\eta}{2}\right)\right. \\ &\left.\times\left[\cos\frac{q_\eta}{2}\cos\frac{q'_\eta}{2} + \cos\frac{q_\eta + q'_\eta}{2}\right]\right)\delta^{pp'},\end{aligned}$$

$$\Lambda^{pp'}_{\delta R\delta\lambda} = \tfrac{1}{2}\delta^{pp'},$$

$$\Lambda^{pp'}_{\delta Rr^\eta} = -\Delta\cos\left(k_\eta - \frac{q_\eta + q'_\eta}{2}\right)\cos\frac{q'_\eta}{2}\delta^{pp'},$$

and

$$\Lambda^{pp'}_{\delta RA^\eta} = \Delta\sin\left(k_\eta - \frac{q_\eta + q'_\eta}{2}\right)\cos\frac{q'_\eta}{2}\delta^{pp'}.$$

Each vertex conserves momentum and energy and they are of $\mathcal{O}(1)$. In each diagram there is a minus sign for each fermion loop and a symmetry factor. Feynman rules are given in figure 2(a).

As usual in a large-N approach, any physical quantity can be calculated at a given order just by counting the powers in $1/N$ of vertices and propagators involved in the corresponding diagrams. In the present summary there is no mention of the ghost fields. They were treated in

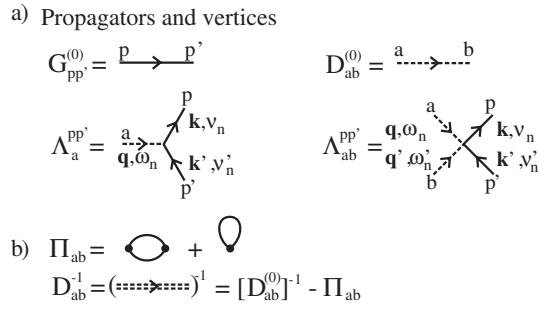

Figure 2. Summary of the Feynman rules. (a) Solid lines represent the propagator $G^{(0)}$ (9). Dashed lines represent the 8×8 boson propagator $D^{(0)}$ (12) for the eight-component field δX^a. Notice that the component (1, 1) of this propagator is directly associated with the X^{00} charge operator. $\Lambda_a^{pp'}$ (13) and $\Lambda_{ab}^{pp'}$ represent the interaction between two fermions f_p and one or two bosons δX^a respectively. (b) Π_{ab} contributions to the irreducible boson self-energy. Double dashed lines correspond to dressed boson propagators.

previous papers [35, 37] and the only role they play is to cancel the infinities given by the two diagrams of figure 2(b).

The exchange interaction J enters (12) in two different channels: (a) the term $2J$ in the element (1, 1) of $D_{(0)}^{-1}$ is due to the charge-like term, $-J/2N \sum_{\langle i,j\rangle;\, pp'} X_i^{pp} X_j^{p'p'}$, of the t–J–V model. This term has the same form as the Coulomb term $V/N \sum_{\langle i,j\rangle;\, pp'} X_i^{pp} X_j^{p'p'}$. (b) The terms $4\Delta^2/J$ in the diagonal of $D_{(0)}^{-1}$ are due to the exchange-like term, $J/2N \sum_{\langle i,j\rangle;\, pp'} X_i^{pp'} X_j^{p'p}$, of the t–J–V model.

In (12) V is only present in the element (1, 1) of $D_{(0)}^{-1}$ and it is multiplied by $(x/2)^2$, which means that it is strongly screened, at low doping, by correlations. In addition, the effect of V is diminished when J is finite.

The bare boson propagator $D_{(0)ab}$ (the inverse of (12)) is $\mathcal{O}(1/N)$. From the Dyson equation, $D_{ab}^{-1} = D_{(0)ab}^{-1} - \Pi_{ab}$, the dressed components D_{ab} (double dashed line in figure 2(b)) of the boson propagator can be found after the evaluation of the 8×8 boson self-energy matrix Π_{ab}. Using the Feynman rules Π_{ab} can be evaluated through the diagrams of figure 2(b). It results as

$$\Pi_{ab}(\mathbf{q}, \mathrm{i}\omega_n) = -\frac{N}{N_\mathrm{s}} \sum_{\mathbf{k}} h_a h_b \frac{\left[n_\mathrm{F}(E_{k+q}) - n_\mathrm{F}(E_k)\right]}{E_{k+q} - E_k - \mathrm{i}\omega_n} - \frac{N}{N_\mathrm{s}} \delta_{a1}\delta_{b1} \sum_{\mathbf{k}} \frac{\varepsilon_{k+q} - \varepsilon_k}{2} n_\mathrm{F}(E_k), \tag{14}$$

where

$$h_a = \Bigg[\frac{\varepsilon_{k+q} + \varepsilon_k}{2}, 1, -2\Delta \cos\left(k_{\eta_1} + \frac{q_{\eta_1}}{2}\right), -2\Delta \cos\left(k_{\eta_2} + \frac{q_{\eta_2}}{2}\right), -2\Delta \cos\left(k_{\eta_3} + \frac{q_{\eta_3}}{2}\right), 2\Delta \sin\left(k_{\eta_1} + \frac{q_{\eta_1}}{2}\right), 2\Delta \sin\left(k_{\eta_2} + \frac{q_{\eta_2}}{2}\right), 2\Delta \sin\left(k_{\eta_3} + \frac{q_{\eta_3}}{2}\right)\Bigg],$$

and $\varepsilon_k = -2t\,(x/2) \sum_\eta \cos(k_\eta)$.

The component (1, 1) of the dressed boson propagator D_{ab} (also called D_{RR}) is related to the charge–charge correlation function χ^{c}_{ij}. It can be written as [35, 41]

$$\chi^{c}_{ij}(\tau) = \frac{1}{N}\sum_{pq}\langle T_\tau X^{pp}_i(\tau) X^{qq}_j(0)\rangle, \tag{15}$$

and the completeness condition and the relation between X^{00}_i and δR_i, in Fourier space,

$$\chi^{c}(\mathbf{q},\omega) = -N\left(\frac{x}{2}\right)^2 D_{RR}(\mathbf{q},\omega). \tag{16}$$

In [35, 37, 41] it was pointed out that in $\mathcal{O}(1)$ the charge–charge correlation function shows the presence of collective peaks above the particle–hole continuum.

Finally, one remark is in order at this point. From the completeness condition (4) we can see that the charge operator X^{00} is of $\mathcal{O}(N)$, while the operators X^{pp} are of $\mathcal{O}(1)$. This fact will have the physical consequence that the $1/N$ approach weakens the effective spin interactions compared to the one related to the charge degrees of freedom. Another consequence of this result is the absence, in $\mathcal{O}(1)$, of collective excitations (like magnons) in the spin susceptibility. The spin–spin correlation function is then a Pauli-like electronic bubble with renormalized band due to correlations [35, 41]. While there are collective effects in the charge sector in $\mathcal{O}(1)$, they appear in $\mathcal{O}(1/N)$ in the spin sector. However, as will be shown in section 4, since superconductivity occurs at relatively large doping where the system behaves as a paramagnetic metal, this fact is not relevant.

3. Phase diagram: instabilities of the homogeneous Fermi liquid

Before considering the possible electronic instabilities, we recall that in leading order we have free fermions with an electronic band E_k (10), renormalized by Coulomb interactions. From this electronic dispersion we obtain a large Fermi surface (FS) enclosing the Γ point. First principles calculations [5] in cobaltates predict, apart from this FS, the existence of small pockets near K points. However, it is important to notice that recent ARPES experiments [6] do not show the presence of pockets. Invoking electronic correlations, a theoretical explanation for the absence of pockets was given using LDA + U [42] and a strong-coupling mean field approach [43]. These results give additional support for considering cobaltates as strongly correlated systems.

Instabilities of the $\mathcal{O}(1)$ HFL phase are studied by analysing the zeros of $\mathrm{Det}\, D^{-1}_{ab} = \mathrm{Det}\,(D^{-1}_{(0)ab} - \Pi_{ab})$. Expanding the determinant by minors along the first row, it can be written in the static limit ($\omega_n = 0$) as follows:

$$\mathrm{Det}\, D^{-1}_{ab} = f(x, J, \mathbf{q})V + g(x, J, \mathbf{q}) \tag{17}$$

where f and g are long algebraic expressions and they were computed numerically in order to study the instabilities. The fact that the Π_{ab}s are V independent functions was used in (17).

The system presents two kinds of instabilities.

(a) *V-dependent instabilities.* They occur when $f \neq 0$. From (17) these instabilities take place for given x, J and $\mathbf{q}$, when the Coulomb potential is $V = V_c = -g/f$.
(b) *V-independent instabilities.* They occur when the two functions f and g are zero simultaneously.

Considering the case for cobaltates where the bare hopping $t \sim 150$ meV [4] and $U_{dd} \sim 3.0$–5.5 eV [8] we obtain, in agreement with other estimates [7, 12], ($J = 4t^2/U$) $J \sim 0.1$–0.2 in units of t. Based on such estimates, we set $J = 0.2$ in what follows.

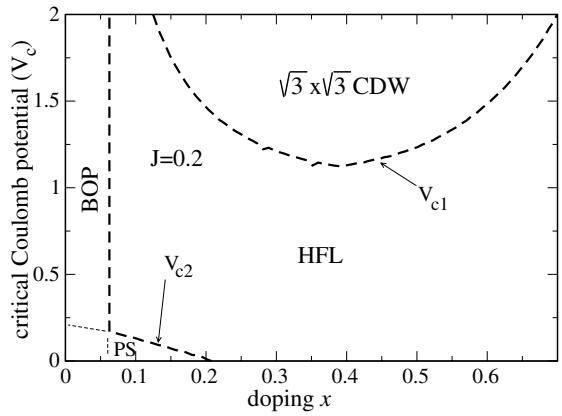

Figure 3. V-dependent phase diagram for $J = 0.2$. V_{c1} marks the border between the HFL and the $\sqrt{3} \times \sqrt{3}$ CDW. V_{c2} marks the border between the HFL and PS. The vertical dashed line separates the HFL from the BOP (see section 3.2).

3.1. Charge density wave instabilities

In this section the stability of the HFL phase will be studied as a function of V, since it corresponds to type (a) above, i.e. to the V-dependent kind. Two instabilities are found with critical values V_{c1} and V_{c2}. In figure 3 we show the phase diagram in the V_c–x plane for $J = 0.2$. Regions corresponding to HFL, $\sqrt{3} \times \sqrt{3}$ CDW ($V > V_{c1}$) and phase separation (PS) ($V < V_{c2}$) are identified.

As usual, PS takes place at $\mathbf{q} = 0$. For a given J, the system shows PS for low x and V below the corresponding line marked with V_{c2}. The PS region increases with increasing J.

When $V > V_{c1}$ the system enters a CDW state. The divergence at the onset of the CDW is at $\mathbf{q} = \mathbf{Q} = (4/3\pi, 0)$ corresponding to a $\sqrt{3} \times \sqrt{3}$ CDW [14, 15]. The V_c–x line separating the HFL from the $\sqrt{3} \times \sqrt{3}$ CDW phase has a parabola-like shape with a minimum closer to the doping $x \sim 0.35$ where superconductivity takes place, with maximum T_c, in cobaltates.

The critical Coulomb repulsion V_{c1} increases with increasing J. As can be seen from the element (1, 1) of $D^{-1}_{(0)ab}$ in (12), the effect of V is diminished by the presence of J. For instance, for $x = 1/3$, V_{c1} is 1 and 1.13 for $J = 0$ and $J = 0.2$, respectively. For $J = 0$ our phase diagram agrees with the obtained one in [14] (see figure 2 of that paper). The eigenvector corresponding to the zero eigenvalue of D^{-1}_{ab} is mainly of the form $(1, 0, 0, 0, 0, 0, 0, 0)$ and therefore the instability is concentrated in the charge sector.

The vertical dashed line separating the HFL from the BOP will be discussed in the next subsection.

3.2. Bond-order phase

This instability corresponds to the V-independent kind. In figure 4 we show the phase diagram of the model considering only this instability. For a given J, below a critical doping x_c, the HFL is unstable. As can be seen, the instability is strongly J dependent. When $J \to 0$, $x_c \to 0$, showing that J is the main source for the instability. For instance, for $J = 0.2$, $x_c \sim 0.066$, which corresponds to the vertical dashed line in figure 3. In the inset of figure 4 we show the J dependence of the critical momentum $\mathbf{q_c}$ where the instability takes place. It is of the form $\mathbf{q_c} = (q_x, 0)$ and leads to an incommensurate instability.

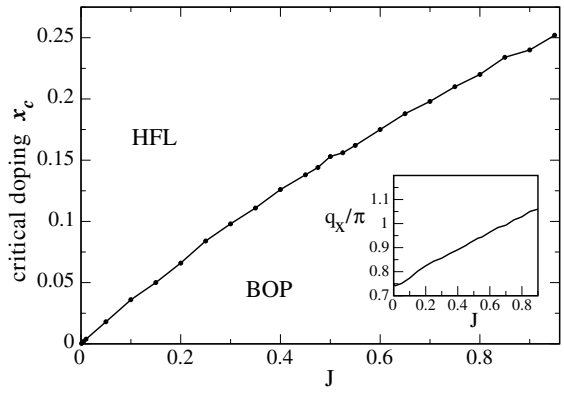

Figure 4. V-independent instability. For a given J the HFL is unstable for $x < x_c$ against the BOP. Inset: q_x versus J.

The dominant symmetry involved in the instability is given by the eigenvector corresponding to the zero eigenvalue, that in this case has the form $\sim(0, 0, 0, -\sqrt{2}/2, \sqrt{2}/2, 0, 0, 0)$, and hence it is in a different sector than the V-dependent instabilities. It means that, for a given J, the amplitude variables r^{η_2} and r^{η_3} of Δ^η (the fourth and fifth components of δX^a) are frozen at $\mathbf{q}_c$ for $x < x_c$. The term $-\Delta \sum_{\langle i,j\rangle,p,\eta}(f^\dagger_{ip} f_{jp} + f^\dagger_{jp} f_{ip}) r^\eta_i$, in the fourth line of our effective Lagrangian (8) (from which the components 3, 4 and 5 of the vertex $\Lambda^{pp'}_a$ (13) are obtained) is, in q-space, of the form $2\Delta \sum_{kqp,\eta} \cos(k_\eta - q_\eta/2) r^\eta_q f^\dagger_{k+q,p} f_{k,p}$. When the variables r^{η_2} and r^{η_3} are frozen, a new hopping-like term of the form $[\cos(q_{cx}/4)\, \mathrm{d}_{xy}(k) + \sin(q_{cx}/4)\mathrm{p}_x(k)]$ is generated in the Hamiltonian. p_x and d_{xy} are harmonics of the triangular lattice [14]. Hence, the instability can be purely of d or p character depending on whether it takes place at $\mathbf{q_c} = (0, 0)$ or $\mathbf{q_c} = (2\pi, 0)$ respectively. In between, both symmetries are mixed. For instance, for $J = 0.2$ we have $\mathbf{q_c} \sim (0.8, 0)\pi$, which means that the instability is $\sim$65% d and $\sim$35% p. Therefore, it is mainly of d-wave character at the onset of the instability. Since in the triangular lattice d-wave symmetry is twofold degenerate, the new phase can be a combination of both.

In the case of the t–J model on the square lattice, these kinds of purely electronic instabilities were studied using SB [44], Bayn–Kadanoff functional theory [45] and the path integral large-N approach [37]. In this case two regimes were obtained. (a) For $J < 0.5$, at low doping the system shows an instability whose eigenvector is mainly confined to the sector corresponding to phase fluctuations A^η_i of the bond variables. Therefore, the new phase has a complex order parameter and corresponds to the well known flux phase (FP). (b) For $J > 0.5$, at low doping the eigenvector of the instability is confined to the sector corresponding to the amplitude variables r^η_i, and hence corresponds to the BOP. This is in fact the order we found in the triangular lattice. From the discussion above, and the fact that phase separation is also found on the triangular lattice, it seems that instabilities expected on the square lattice at high values of J already appear at low values on the triangular lattice, a feature that may be due to the larger coordination number. We would like to point out that, to our knowledge, this kind of analysis has not been done before for the t–J model on the triangular lattice.

Finally, a word of caution about the BOP is in place here. Our figure 4 shows that at zero doping the BOP would set in for finite J. However, numerical results [46, 47] indicate that the antiferromagnetic Heisenberg model on a triangular lattice displays long-range Néel order for spin $S = 1/2$. The same discrepancy appears on the square lattice with the techniques mentioned above. While, due to its bipartite nature, the antiferromagnetic order is expected to

be rather robust on a square lattice, geometric frustration on the triangular lattice should render this state much more fragile, such that, upon doping, RVB-like scenarios [3] appear even more probable in the present case. Therefore, since our large-N approach shows phases like the FP and BOP at low doping on a square lattice [37], as do other mean field approaches (see above), that are considered as serious candidates for underdoped cuprates, we expect the results on the triangular lattice to be even more trustworthy.

4. Superconductivity

Having studied the stability conditions for the HFL under the influence of V and J, we consider in this section possible superconducting states.

In [15] we have proposed that the interplay between electronic correlations and e–ph interaction may be important for describing superconductivity in cobaltates. With this aim we consider the additional electron–phonon Hamiltonian $H_{\rm ph} + H_{\rm e-ph}$, where

$$H_{\rm ph} = \sum_i \omega_{\rm E} \left(a_i^\dagger a_i + \tfrac{1}{2} \right), \tag{18}$$

and

$$H_{\rm e-ph} = \frac{g}{\sqrt{N}} \sum_{i,p} (a_i^\dagger + a_i) X_i^{pp}. \tag{19}$$

In order to obtain a finite theory in the $N \to \infty$ we have rescaled the e–ph coupling g to $g/\sqrt{N}$.

From $H_{\rm ph}$ (18) we have a free phonon propagator

$$D_0^{\rm ph} = \frac{-2\omega_{\rm E}}{\omega_n^2 + \omega_{\rm E}^2}, \tag{20}$$

which is of $\mathcal{O}(1)$. Using the constraint (5), the expression (19) for $H_{\rm e-ph}$ reads

$$H_{\rm e-ph} = \frac{g}{\sqrt{N}} \sum_{ip} (a_i^\dagger + a_i) \frac{f_{ip}^\dagger f_{ip}}{(1 + \delta R_i)}, \tag{21}$$

where the relations between X^{0p} and f_p and between X^{00} and δR were also used. Up to $\mathcal{O}(1/N)$ only the first term in the expansion of $1/(1 + \delta R)$ is necessary, leading to

$$H_{\rm e-ph} = \frac{g}{\sqrt{N}} \sum_{ip} (a_i^\dagger + a_i)(1 - \delta R_i) f_{ip}^\dagger f_{ip}. \tag{22}$$

Next, we discuss the effective interaction between carriers. Fluctuations in $\mathcal{O}(1/N)$ give rise to interactions among fermions. In $\mathcal{O}(1/N)$ there are two contributions to the total pairing effective potential $V_{\rm eff}^{\rm T}$ shown in figure 5(a). The first diagram of figure 5(a) shows the pairing effective potential, $V_{\rm eff}^{t-J-V}$, for the pure t–J–V model while the second diagram shows the e–ph pairing potential $V_{\rm eff}^{\rm e-ph}$. Notice that $1/N$ self-energy corrections in the fermionic propagator (9) are not necessary for calculating $V_{\rm eff}$ in $\mathcal{O}(1/N)$.

Due to the rescaling of the e–ph interaction, g, superconductivity from phonons also appears in $\mathcal{O}(1/N)$, and therefore it can be treated on an equal footing to superconductivity in the pure t–J–V model.

The new contribution to the e–ph pairing potential is the vertex (dark triangle) in the second diagram of figure 5(a) which represents the e–ph interaction renormalized by electronic correlations. The diagram of figure 5(b) shows that the renormalization of the bare vertex g is due to the electronic correlations of the pure t–J–V model, which will be the main contribution

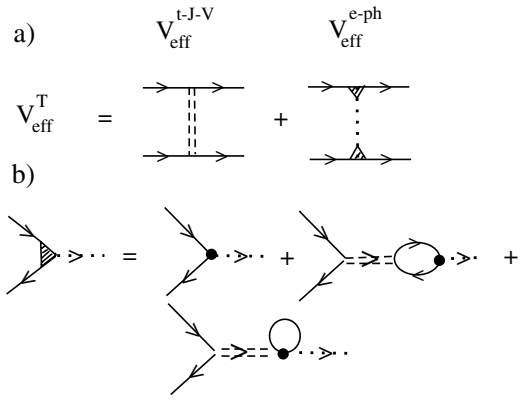

Figure 5. (a) Total effective pairing $V_{\rm eff}^{\rm T}$ as the sum of a pure electronic mediated $V_{\rm eff}^{t-J-V}$ and a phonon mediated $V_{\rm eff}^{\rm e-ph}$ interactions. Solid, double dashed and dotted lines are the propagators for fermions, D_{ab} and phonons respectively. In $V_{\rm eff}^{\rm e-ph}$, the bare e–ph vertex, g (solid circle), is renormalized by electronic correlations as shown in (b). The last diagram contains a four-leg vertex proportional to g, which is generated when our X-operator approach is applied (see (22)).

to our results. Notice that the e–ph vertex is not renormalized by the e–ph interaction. Hence, we assume, as in usual metals, that Migdal theorem is valid.

Using our Feynman rules the renormalized e–ph vertex γ is

$$\gamma(q,k',k'',\omega_n,\nu_n',\nu_n'') = gN\left(\frac{x}{2}+2\Delta\frac{1}{N_{\rm s}}\sum_{k,\eta}\cos\frac{q_\eta}{2}\cos\left(k+\frac{q}{2}\right)_\eta\frac{[n_{\rm F}(E_{k+q})-n_{\rm F}(E_k)]}{E_{k+q}-E_k-{\rm i}\omega_n}\right)$$
$$\times\, D^{Rb}(q,\omega_n)\Lambda_b^{pp}, \tag{23}$$

where Λ_b^{pp} is given by (13).

In the $J=0$ case, the renormalized e–ph vertex can be written as

$$\gamma(q,k',k'',\omega_n,\nu_n',\nu_n'') = Ng\frac{x}{2}\left\{\left[\frac{\rm i}{2}(\nu_n'+\nu_n'')+\mu\right]D_{RR}(q,\omega_n)+D_{\lambda R}(q,\omega_n)\right\}, \tag{24}$$

where the relevant contribution comes from the charge–charge correlation D_{RR} (16). Vertex corrections obtained by us are similar to the early calculations of [48], which were used before for studying transport [49] and the isotope effect in cuprates [50].

In weak coupling we can evaluate the effective interactions on the FS, i.e. for $\omega_n=\nu_n'=\nu_n''=0$ and the momentum $\mathbf{q}=\mathbf{k}-\mathbf{k}'$ with $\mathbf{k}$ and $\mathbf{k}'$ on the FS. Then, the total pairing effective potential is

$$V_{\rm eff}^{\rm T}(\mathbf{k},\mathbf{k}') = V_{\rm eff}^{t-J-V}(\mathbf{k},\mathbf{k}')+V_{\rm eff}^{\rm e-ph}(\mathbf{k},\mathbf{k}'), \tag{25}$$

where, using the Feynman rules,

$$V_{\rm eff}^{t-J-V}(\mathbf{k},\mathbf{k}') = \Lambda_a^{pp}D^{ab}(\mathbf{k}-\mathbf{k}')\Lambda_b^{pp}, \tag{26}$$

and

$$V_{\rm eff}^{\rm e-ph}(\mathbf{k},\mathbf{k}') = -\frac{\lambda}{N(0)}\left[\gamma^*(\mathbf{k},\mathbf{k}')\right]^2, \tag{27}$$

where $\lambda=\frac{2g^2}{\omega_{\rm E}}N(0)$ is the bare dimensionless e–ph coupling and $N(0)$ is the bare electronic density of states. In (27) $\gamma^*=\gamma/g$.

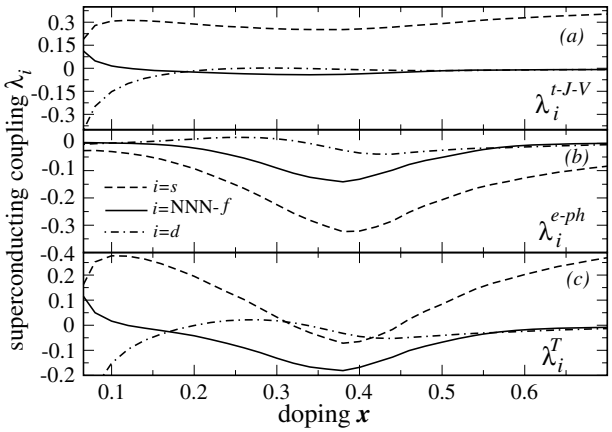

Figure 6. Superconducting couplings λ_i in the s (dashed line), d (dotted-dashed line) and NNN-f (solid line) channels for (a) the pure t–J–V model, (b) the e–ph model and (c) the total case. Results are for $J = 0.2$ and $V = 0.9V_c$, which locates the system near the $\sqrt{3} \times \sqrt{3}$ CDW phase. The bare e–ph superconducting coupling was chosen to be $\lambda = 0.4$.

In the following we choose $\lambda = 0.4$. To our knowledge the value of λ is not known for cobaltates yet. However, recent experiments suggest that it is non-negligible [51]. $\lambda = 0.4$ is of the order of recent estimates [52, 53].

Without correlations, $\gamma^* = 1$ and $V_{\text{eff}}^{\text{e-ph}}$ is the usual pairing potential used in BCS theory, which in conventional metals leads to superconductivity in the isotropic s-wave channel. However, in such a case, the characteristic dome shape observed in cobaltates would not be expected, because there is no reason for a strongly doping dependent bare e–ph coupling λ. Recently, Yada and Kontani [52], using a d–p model for $NaCoO_2$, found evidence for phonon mediated superconductivity in the s-wave channel, so that, as they pointed out, other effects, such as electronic correlations, are necessary in order to stabilize an anisotropic pairing.

We use the effective potentials to compute the dimensionless effective couplings in the different pairing channels or irreducible representations of the order parameter. The critical temperatures T_c can be then estimated from $T_{ci} = 1.13\omega_c \exp(1/\lambda_i)$, where ω_c is a suitable cut-off frequency.

The effective couplings λ_i with different symmetries are defined as [36]

$$\lambda_i = \frac{1}{(2\pi)^2} \frac{\int (\mathrm{d}\mathbf{k}/|v_{\mathbf{k}}|) \int (\mathrm{d}\mathbf{k}'/|v_{\mathbf{k}'}|) g_i(\mathbf{k}') V_{\text{eff}}(\mathbf{k}', \mathbf{k}) g_i(\mathbf{k})}{\int (\mathrm{d}\mathbf{k}/|v_{\mathbf{k}}|) g_i(\mathbf{k})^2} \tag{28}$$

where the functions $g_i(\mathbf{k})$ encode the different pairing symmetries (see table 1 of [14] for the triangular lattice), and $v_{\mathbf{k}}$ are the quasiparticle velocities at the Fermi surface. The integrations are restricted to the Fermi surface. λ_i measures the strength of the interaction between electrons at the Fermi surface in a given symmetry channel i. If $\lambda_i > 0$, electrons are repelled. Hence, superconductivity is only possible when $\lambda_i < 0$.

Figure 6 shows results for the most relevant symmetry channels as s, d and NNN-f for $J = 0.2$ and $V \sim 1$ close to the $\sqrt{3} \times \sqrt{3}$ CDW (see figure 3). The curves were cut at $x \sim 0.066$, where the BOP instability takes place. Figure 6(a) corresponds to the pure t–J–V model. As expected, $\lambda_s^{t-J-V} > 0$ (dashed line), hence electrons are repelled, indicating no tendencies to superconductivity with s symmetry.

In the NNN-f channel (solid line) we have obtained small negative values for $\lambda_{\text{NNN-f}}^{t-J-V}$ with a shallow minimum around $x \sim 0.38$, suggesting the possibility of superconductivity.

However, in the most favourable case $\lambda^{t-J-V}_{\text{NNN-f}} \sim -0.04$, implying that an unrealistic cut-off ω_c is necessary in order to obtain a value of a few kelvin for T_c. This feature remains valid even closer to the $\sqrt{3} \times \sqrt{3}$ CDW phase.

The dotted–dashed line shows results for λ^{t-J-V}_{d}. Negative superconducting couplings are found at small doping, $x < 0.15$, where λ^{t-J-V}_{d} can take robust values ~ -0.3, indicating that superconductivity in the d-wave channel may be expected at such low doping. Our calculations show that λ^{t-J-V}_{d} is independent of V. On the other hand, λ^{t-J-V}_{d} is strongly J dependent, vanishing fast when $J \to 0$. Comparing figures 3 and 6, it can be seen that d-wave superconductivity occurs near the onset of BOP, which is also of d-wave character and triggered by J. For the doping range where superconductivity takes place in cobaltates, $x \sim 0.35$, there is no indication for d-wave pairing.

Figure 6(b) shows results for the e–ph case. $\lambda^{\text{e-ph}}_{\text{s}}$ (dashed line) would suggest that superconductivity could be expected in the s-wave channel around $x \sim 0.38$ following a dome shape as in cobaltates. However, in a Gutzwiller description the s-wave order parameter would be exactly zero. In contrast to that, the enforcement of the large-N non-double occupancy constraint (4), namely, that only $N/2$ out of the total N states at a given site can be occupied at the same time, makes s-wave superconductivity possible in spite of strong correlations (see [50] for discussions).

$\lambda^{\text{e-ph}}_{\text{NNN-f}}$ (solid line) shows robust negative superconducting couplings following a dome shape around $x \sim 0.38$. Notice that $\lambda^{\text{e-ph}}_{\text{NNN-f}} \sim -0.16$, which is a factor of four larger than for the pure t–J–V model. NNN-f superconductivity is not very sensitive to the value of J and the only requirement is that the system must be close to a charge instability (in this case a $\sqrt{3} \times \sqrt{3}$ CDW).

The dotted–dashed line in figure 6(b) shows the projection of the e–ph coupling on the d-wave channel, $\lambda^{\text{e-ph}}_{d}$. In the uncorrelated case $\lambda^{\text{e-ph}}_{d}$ is exactly zero, but electronic correlations are responsible for the weak modulation with doping of $\lambda^{\text{e-ph}}_{d}$. For low doping, $\lambda^{\text{e-ph}}_{d}$ can take small but negative values of the order of $\lambda^{\text{e-ph}}_{d} \sim -0.02$ (not well appreciated in the scale of figure 6). These small and negative values for $\lambda^{\text{e-ph}}_{d}$ increase with J. An appreciable strength of $\lambda^{\text{e-ph}}_{d}$ can only be obtained for unrealistic values of J. As we mentioned above the renormalized e–ph vertex is mainly dominated by charge fluctuations, and then NNN-f pairing proves correlation effects better than d-wave pairing.

Figure 6(c) shows results for the total coupling $\lambda^{\text{T}}_{i} = \lambda^{t-J-V}_{i} + \lambda^{\text{e-ph}}_{i}$. The solid line ($\lambda^{\text{T}}_{\text{NNN-f}}$) shows the strongest tendencies to superconductivity. The dome shape around $x \sim 0.38$ is clearly present. While $\lambda^{t-J-V}_{\text{NNN-f}}$ is small but negative, $\lambda^{\text{T}}_{\text{NNN-f}}$ increases slightly with respect to $\lambda^{\text{e-ph}}_{\text{NNN-f}}$.

The situation is different for the s-wave channel; as $\lambda^{t-J-V}_{\text{s}} > 0$, $\lambda^{\text{T}}_{\text{s}}$ will be smaller than $\lambda^{\text{e-ph}}_{\text{s}}$. For instance, $\lambda^{\text{T}}_{\text{s}} \sim -0.05$ at $x \sim 0.38$, as a result of strong correlations.

Finally, as the contribution $\lambda^{\text{e-ph}}_{d}$ (dotted–dashed line in panel (b)) is very small, the total effective coupling λ^{T}_{d} is close to λ^{t-J-V}_{d}. In the triangular lattice the d-wave channel is degenerate. Our calculation determines the leading symmetry of the superconducting order parameter but not its value. However, our results are consistent with previous mean field studies [10, 12] where superconductivity was found with $\text{d}_1 + \text{id}_2$ symmetry. We would like to remark that these mean field studies assume the pure J term as the effective interaction. In our calculation we have included fluctuations through the infinite series of bubbles in the evaluation of the propagator D_{ab}.

We conclude that the t–J–V model alone would support superconductivity in the d-wave channel at low doping ($x < 0.15$ for $J = 0.2$). To our knowledge there are at present no

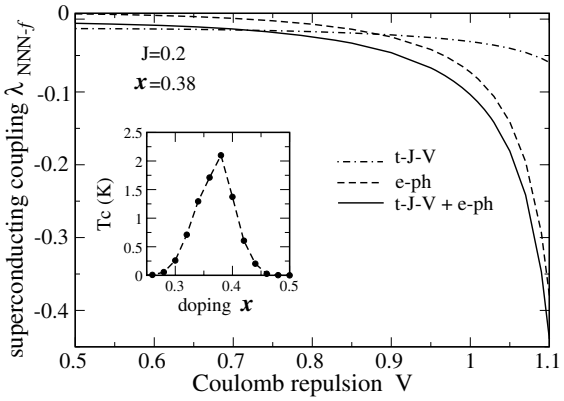

Figure 7. Superconducting coupling in the NNN-f channel as a function of V approaching the critical value V_c for $J = 0.2$. The figure is presented for $x = 0.38$ where the largest superconducting coupling was obtained. Results for the pure t–J–V model (dotted–dashed line), pure e–ph model (dashed line) and the total case (solid line) are presented, showing that, when phonons are included, a large window near the $\sqrt{3} \times \sqrt{3}$ CDW phase exists where the system presents indications for superconductivity. Inset: T_c versus doping for the NNN-f channel. The BCS formula was used for the estimation of T_c (see text).

data for such doping levels concerning superconductivity. On the other hand, while e–ph interaction essentially introduces no changes in the d-wave channel, it effectively couples to charge fluctuations close to a charge ordering instability. Near charge order, charge fluctuations renormalize the e–ph effective interaction in such a way that superconductivity with triplet NNN-f symmetry is favoured around $x \sim 0.38$.

In order to see the influence of the proximity to the charge order on superconductivity, in figure 7 we show, for $x = 0.38$, the values of $\lambda^{t-J-V}_{\text{NNN-f}}$ (dotted–dashed line), $\lambda^{\text{e-ph}}_{\text{NNN-f}}$ (dashed line) and $\lambda^{\text{T}}_{\text{NNN-f}}$ (solid line) as a function of V. For the pure t–J–V model the values of $\lambda^{t-J-V}_{\text{NNN-f}}$ are very small even very close to the $\sqrt{3} \times \sqrt{3}$ CDW. In contrast, when e–ph interaction is included, there is a large window for the parameters for which superconductivity may be possible. As $\lambda^{\text{T}}_{\text{NNN-f}}$ increases with V, T_c will also increase. For cobaltates, it is known from experiments that T_c increases with water inclusion [55], supporting the view that the increasing of V mimics the increasing of water content. For small V, $\lambda^{\text{T}}_{\text{NNN-f}}$ is very small, in agreement with the non-existence of superconductivity in nonhydrated samples.

Although at this point a quantitative comparison with experiments is beyond the scope of our analysis, it is still of interest to make a qualitative estimate of T_c. Since NNN-f superconductivity is in our case mainly mediated by phonons, we consider as a relevant cut-off the corresponding energy scale. Recent first principles lattice dynamics calculations [54] show the existence of optical phonons as high as 75 meV, and for simple estimates we consider $\omega_E = 40$ meV [53]. Using the values for $\lambda^{\text{T}}_{\text{NNN-f}}$ (solid line in panel (c) of figure 6) we show, in the inset of figure 7, results for T_c. Our crude estimate gives $T_c \sim 2$ K, which is of the order of the experimental value $T_c \sim 5$ K. *A priori*, this result may appear trivial because the e–ph interaction is certainly efficient for leading to superconductivity with T_c in the scale of a few kelvin in usual metals. However, there are two features in our results that would be absent when correlations are left aside. First, the pairing channel is an unconventional one, a result that would not be possible considering e–ph interaction alone. Second, a dome shape is obtained for T_c, again a fact that would be missing by considering e–ph interaction alone.

5. Conclusions and discussions

We have studied the t–J–V model plus phonons on the triangular lattice.

Before studying superconductivity we have presented the phase diagram of the model. Two types of instabilities were found. (a) V-dependent instabilities. These instabilities are dominated by the short-range Coulomb repulsion V. For V larger than a critical value V_c the system enters a $\sqrt{3} \times \sqrt{3}$ CDW phase. PS was also obtained for small x and V. (b) V-independent instability. This instability is dominated by J and is common to the pure t–J model. For a given J, the system is unstable for doping smaller than a critical one x_c. This new phase occurs at an incommensurate momentum q_c and it is called BOP. It was found that $x_c \to 0$ when $J \to 0$.

These phases delimit the region of parameters (x, J and V) where the HFL is stable. Paring was calculated in this last region.

Near the $\sqrt{3} \times \sqrt{3}$ CDW state the e–ph vertex is renormalized by electronic correlations developing an anisotropy in k-space due to the coupling with charge fluctuations. This anisotropy favours superconductivity with NNN-f symmetry when the renormalized vertex is used for calculating phonon mediated pairing. Besides the possibility of anomalous pairing, the model shows possible superconductivity following a dome shape around $x \sim 0.35$ with values for T_c of the order of a few kelvin. We have found that the above results are robust against the value of J around $x \sim 0.35$.

In addition to NNN-f superconductivity for doping $x \sim 0.35$, for finite J we have found the possibility of d-wave pairing at low doping. For instance, for $J = 0.2$, on the high side for possible values of J, d-wave pairing can be expected for $x < 0.15$. In contrast to NNN-f pairing, d-wave pairing is not affected by V, suggesting that superconductivity in that channel could exist even without hydration. To our knowledge superconductivity was not investigated in cobaltates for samples at such small doping levels.

A discussion in relation to cobaltates is in order at this point. It was recently proposed [56], and studied experimentally [55], that hydration causes the electronic structure to be more two dimensional. Notice that in [55] it was shown that T_c decreases with decreasing lattice parameter c. We think that due to this effect the Coulomb repulsion V may be less screened when the system is hydrated. If V is small when the system is not hydrated, phonons will favour superconductivity only in the s-wave channel. However, the strong repulsion in this channel from the t–J–V model (figure 6(a)) suppresses pairing from phonons. This may be the reason for the nonexistence of superconductivity in non-hydrated cobaltates.

As NNN-f superconductivity has a large contribution from phonons we expect a large isotope coefficient. Our theory also predicts a rather constant isotope coefficient along the dome in contrast to the strong doping dependent isotope coefficient in cuprates [57]. To our knowledge, isotope effect experiments are still not available for cobaltates. We expect that the improvement in single-crystal preparation [58] will be useful for isotope experiments in the near future. We consider this experiment as a strong test for our approach.

We would like to remark about some analogies between cobaltates and organic materials. As in organic materials [59], optical conductivity experiments in cobaltates [60] show the presence of low-energy features which can be associated with the proximity of the system to the charge order. Merino and McKenzie [61] pointed out that the proximity to the charge order is relevant for superconductivity with anomalous paring in organic systems. As our scenario predicts a $\sqrt{3} \times \sqrt{3}$ CDW state for $V > V_c$ it will be interesting to see if a further inclusion of water can trigger the $\sqrt{3} \times \sqrt{3}$ CDW phase or, at least, if low-energy optical features are reinforced with hydration.

Recent reports discuss the possibility for singlet s-wave superconductivity [27] and the coexistence of s-wave and unconventional pairing [62]. Such a situation could be reached in our case by increasing the bare λ from $\lambda = 0.4$, since then the total superconducting couplings λ_s^T and $\lambda_{NNN\text{-}f}^T$ become more attractive and, for $\lambda > 1$, both symmetries are nearly degenerate. However, lacking detailed information about the e–ph coupling, we take a cautious value for λ, that is already sufficient to trigger superconductivity, and as shown above of unconventional type.

Acknowledgments

The authors thank J Merino and Y Krockenberger for valuable discussions. M Bejas thanks DAAD for financial support and the University of Stuttgart for hospitality.

References

[1] Takada K, Sakurai H, Takayama-Muromachi E, Izumi F, Dilanian R A and Sasaki T 2003 *Nature* **422** 53–5
[2] Schaak R E, Klimczuk T, Foo M L and Cava R J 2003 *Nature* **424** 527–9
[3] Anderson P W 1987 *Science* **235** 1196
[4] Singh D J 2000 *Phys. Rev.* B **61** 13397–402
[5] Singh D J 2003 *Phys. Rev.* B **68** 020503(R)
[6] Hasan M Z *et al* 2004 *Phys. Rev. Lett.* **92** 246402
[7] Yang H B *et al* 2004 *Phys. Rev. Lett.* **92** 246403
[8] Chainani A *et al* 2004 *Phys. Rev.* B **69** 180508(R)
[9] Baskaran G 2003 *Phys. Rev. Lett.* **91** 097003
[10] Kumar B and Shastry B S 2003 *Phys. Rev.* B **68** 104508
[11] Kumar B and Shastry B S 2004 *Phys. Rev.* B **69** 059901(E)
[12] Wang Q H, Lee D H and Lee P A 2004 *Phys. Rev.* B **69** 092504
[13] Tanaka Y, Yanase Y and Ogata M 2004 *J. Phys. Soc. Japan* **73** 319–22
[14] Motrunich O I and Lee P A 2004 *Phys. Rev.* B **70** 024514
[15] Foussats A, Greco A, Bejas M and Muramatsu A 2005 *Phys. Rev.* B **72** 020504(R)
[16] Tanaka A and Hu X 2003 *Phys. Rev. Lett.* **91** 257006
[17] Kuroki K, Tanaka Y and Arita R 2004 *Phys. Rev. Lett.* **93** 077001
[18] Mochizuki M, Yanase Y and Ogata M 2005 *Phys. Rev. Lett.* **94** 147005
[19] Khaliullin G, Koshibae W and Maekawa S 2004 *Phys. Rev. Lett.* **93** 176401
[20] Yanase Y, Mochizuki M and Ogata M 2005 *J. Phys. Soc. Japan* **74** 2568
[21] Yanase Y, Mochizuki M and Ogata M 2005 *J. Phys. Soc. Japan* **74** 3351
[22] Fujimoto T *et al* 2004 *Phys. Rev. Lett.* **92** 047004
[23] Kato M *et al* 2006 *J. Phys.: Condens. Matter* **18** 669
[24] Ihara Y *et al* 2006 *J. Phys. Soc. Japan* **75** 013708
[25] Kanigel A *et al* 2004 *Phys. Rev. Lett.* **92** 257007
[26] Higemoto W *et al* 2004 *Phys. Rev.* B **70** 134508
[27] Kobayashi Y, Yokoi M and Sato M 2003 *J. Phys. Soc. Japan* **72** 2453
[28] Yang H D *et al* 2005 *Phys. Rev.* B **71** 020504(R)
[29] Mazin I I and Johannes M D 2005 *Nat. Phys.* **1** 91–3
[30] Shimojima T *et al* 2005 *Phys. Rev.* B **71** 020505
[31] Lemmens P *et al* 2006 *Phys. Rev. Lett.* **96** 167204
[32] Qian D *et al* 2006 *Phys. Rev. Lett.* **96** 216405
[33] Ning F L and Imai T 2005 *Phys. Rev. Lett.* **94** 227004
[34] Hubbard J 1963 *Proc. R. Soc.* A **276** 238
[35] Foussats A and Greco A 2002 *Phys. Rev.* B **65** 195107
[36] Merino J, Greco A, McKenzie R H and Calandra M 2003 *Phys. Rev.* B **68** 245121
[37] Foussats A and Greco A 2004 *Phys. Rev.* B **70** 205123
[38] Greco A, Merino J, Foussats A and McKenzie R H 2005 *Phys. Rev.* B **71** 144502
[39] Lee P A, Nagaosa N and Wen X G 2006 *Rev. Mod. Phys.* **78** 17
[40] Foussats A, Greco A, Repetto C, Zandron O P and Zandron O S 2000 *J. Phys. A: Math. Gen.* **33** 5849–66

[41] Gehlhoff L and Zeyher R 1995 *Phys. Rev.* B **52** 4635
[42] Zhang P, Luo W, Cohen M and Louie S 2004 *Phys. Rev. Lett.* **93** 236402
[43] Zhou S *et al* 2005 *Phys. Rev. Lett.* **94** 206401
[44] Morse D and Lubensky T 1990 *Phys. Rev.* B **42** 7994
[45] Cappelluti E and Zeyher R 1999 *Phys. Rev.* B **59** 6475
[46] Bernu B, Lhuillier C and Pierre L 1992 *Phys. Rev. Lett.* **69** 2590
[47] Capriotti L, Trumper A E and Sorella S 1999 *Phys. Rev. Lett.* **82** 3899
[48] Kulić M and Zeyher R 1994 *Phys. Rev.* B **49** 4395
[49] Zeyher R and Kulić M 1996 *Phys. Rev.* B **53** 2850
[50] Greco A and Zeyher R 1999 *Phys. Rev.* B **60** 1296
[51] Lupi S, Ortolani M and Calvani P 2004 *Phys. Rev.* B **69** 180506
[52] Yada K and Kontani H 2006 *J. Phys. Soc. Japan* **75** 033705
[53] Rueff J P *et al* 2006 *Phys. Rev.* B **74** 020504(R)
[54] Li Z, Yang J, Hou J and Zhu Q 2004 *Phys. Rev.* B **70** 144518
[55] Sakurai H *et al* 2004 *J. Phys. Soc. Japan* **73** 2590
[56] Marianetti C, Kotliar G and Ceder G 2004 *Phys. Rev. Lett.* **92** 196405
[57] Frank J 1994 *Physical Properties of High-Temperature Superconductors IV* ed D M Ginsberg (Singapore: World Scientific)
[58] Krockenberger Y, Fritsch I, Cristiani G, Matveev A, Alff L, Habermeier H U and Keimer B 2005 *Appl. Phys. Lett.* **86** 191913
[59] Dressel M, Drichko N, Schlueter J and Merino J 2003 *Phys. Rev. Lett.* **90** 167002
[60] Hwang J, Yang J, Timusk T and Chou F 2005 *Phys. Rev.* B **72** 024549
[61] Merino J and McKenzie R H 2001 *Phys. Rev. Lett.* **87** 237002
[62] Chen Y J *et al* 2005 *Preprint* cond-mat/0511385